

# Correlating Hardness Retention and Phase Transformations of Al and Mg Cast Alloys for Aerospace Applications

W. Kasprzak, F. Czerwinski, M. Niewczas, and D.L. Chen

(Submitted October 19, 2014; in revised form December 6, 2014; published online January 22, 2015)

The methodology based on correlating hardness and phase transformations was developed and applied to determine the maximum temperature of hardness retention of selected Al-based and Mg-based alloys for aerospace applications. The Al alloys: A356, F357, and C355 experienced 34–66% reduction of the initial hardness, in comparison to 4–22% hardness reduction observed in Mg alloys: QE22A, EV31A, ZE41A, and WE43B after the same annealing to 450 °C. For Al alloys the hardness reduction showed a steep transition between 220 and 238 °C. In contrast, Mg alloys showed a gradual hardness decrease occurring at somewhat higher temperatures between 238 and 250 °C. The hardness data were correlated with corresponding phase transformation kinetics examined by dilatometer and electrical resistivity measurements. Although Mg alloys preserved hardness to higher temperatures, their room temperature tensile strength and hardness were lower than Al alloys. The experimental methodology used in the present studies appears to be very useful in evaluating the softening temperature of commercial Al- and Mg-based alloys, permitting to assess their suitability for high-temperature applications.

**Keywords** Al/Mg cast alloys, dilatometer, electrical resistivity, hardness retention, mechanical properties, phase transformation

## 1. Introduction

The lightweight Al- and Mg-based cast alloys represent key engineering materials for structural aerospace applications due to their superior strength to weight ratio, corrosion resistance, and castability. Both groups of alloys offer advantages and challenges with respect to their in-service performance characteristics, easiness of manufacturing, and associated costs. For both groups of alloys the precision sand casting process is used to produce low-volume, highly complex-shaped parts with a high level of structural integrity. The desired microstructure with controlled and predictable internal porosity is achieved via combination of the mold design, liquid metal treatment, and directional solidification, combined with the core chill technology (Ref 1). The castability requirements of these alloys represent the significant factor to ensure that chemistry modifications, required to achieve the desired structural characteristics, do not impair the mold-filling ability and quality of the final cast part.

The A356, F357, and C355 Al alloys are key candidates for a variety of structural and powertrain applications. There is a

growing demand to develop a new class of alloys for high-temperature performance, because the operating temperature of existing alloys, typically below 180 °C, is not sufficient for new applications. For example, the accessory gear box used in jet engines requires service temperatures during continuous and peak operating conditions exceeding 170 and 250 °C, respectively (Ref 2), making alloys such as C355 not suitable for these components. Similar demands are observed in the automotive powertrain systems; for example, the engine block development is constantly challenged to increase power density, i.e., to obtain more power from the same or lower alloy weight. This is achieved by increasing the operating temperature at higher compression rates, underlining the need for improved fatigue resistance and creep strength of the alloys up to 250 °C (Ref 3, 4).

The Mg alloys have several important characteristics, which include low density (30% lower than Al alloys), high specific strength, dimensional stability, and good machinability. Despite these advantages, Mg alloys have not been a primary choice for structural parts in powertrain due to their poor elevated temperature properties, low stiffness, and high surface reactivity (Ref 5, 6). In automotive engine components, where channeling coolant or running surfaces are of concern, in addition to low modulus of elasticity, the insufficient corrosion resistance is the major drawback. To overcome these limitations, Al/Mg composites have been explored in applications for automotive engine blocks and crankcases (Ref 7). In this design, the cylinder running surface, the cooling water jacket, cylinder head studs, and main bearings are made from Al alloy, inserted in the Mg-alloy matrix, reducing the weight by 24% in comparison to all Al-alloy design. For aerospace applications the family of cast Mg-based alloys including the QE22A, EV31A, ZE41A, and WE43B grades with improved high-temperature performance, achieved via additions of rare earth elements, was introduced for components requiring service temperature up to 250 °C.

W. Kasprzak and F. Czerwinski, CanmetMATERIALS, Natural Resources Canada, 183 Longwood South St., Hamilton, ON, Canada; M. Niewczas, McMaster University, 1280 Main St. West, Hamilton, ON, Canada; and D.L. Chen, Ryerson University, 350 Victoria Street, Toronto, ON, Canada. Contact e-mails: wojciech.kasprzak@nrcan.gc.ca and wkasprza@nrcan.gc.ca.

To meet higher demands for in-service operating parameters of automotive and aerospace components at elevated temperatures, better understanding of the relationship between mechanical, structural, and thermo-physical properties of the alloys is required. This knowledge is paramount since improvements in the material performance achieved during the last few decades were mostly associated with an increase in understanding and development of complex relationships between composition, processing, microstructure, and properties (Ref 8). Such data represent the fundamental knowledge that can be used to develop new high performance materials, with Al- and Mg-based alloys being the primary candidates.

The alloy hardness can be used as an indicator of its performance at temperatures up to 500 °C. The hardness characteristics obtained during isochronal annealing experiments have been used to evaluate phase transformation kinetics during alloy aging, to determine the aging parameters required to activate specific types of precipitates. Such methodology was used by Knipling et al. (Ref 9) to analyze aging transformation kinetics of synthetic Al-Zr-Ti model alloys. While hardness and microstructure evolution have often been discussed in the literature, the corresponding phase transformations have seldom been analyzed by means of thermo-physical methods. Vlach et al. (Ref 10) used isochronal annealing with a combination of microhardness, electrical resistivity, and differential scanning calorimetry to evaluate the effect of small additions of Sc and Zr on microstructure along with thermodynamic and mechanical properties of Al-Sc-Zr mold cast and cold-rolled cast alloys. Other studies have reported on using dilatometry, electrical resistivity, and/or differential scanning calorimetry in a separate set of experiments (Ref 11).

The aim of this study was the comparative analysis of hardness retention and corresponding phase transformations in Al-based and Mg-based alloys, in the temperature range between 25 and 450 °C. The maximum temperature the alloys can withstand without drastic loss of hardness was determined and correlated with the corresponding phase transformation data to develop the methodology for an assessment of the alloy's high-temperature performance. The hardness retention

capabilities were also compared with initial properties of tested alloys at room temperature.

## 2. Experimental Procedure

### 2.1 Material and Characterization Techniques

Al-based A356, F357, and C355 alloys and Mg-based QE22A, EV31A, ZE41A, and WE43B alloys with potential applications for high integrity and high precision sand cast aerospace components intended for elevated temperature service have been used in the present studies. Test coupons, with chemistries specified in Tables 1 and 2, in the form of tensile test bars, were cast using the ASTM: B108/B108 M-12e1 mold. All concentrations of alloying elements discussed throughout this work are expressed in weight percent unless specified otherwise. The alloy melting and liquid metal processing as well as casting of test coupons were done as per appropriate standard specifications. After casting, the test coupons were subjected to T6 or T5 heat treatments following the ASTM standard to meet the temper requirements, as per commercial production procedures. Details of alloy conditions, processing parameters, and testing are summarized in Table 3.

The alloy hardness was measured at room temperature using a Buehler Rockwell tester employing F scale and 60 kg load. For each sample, twenty measurements were conducted and an average value along with the standard deviation was plotted. The hardness retention as a function of the temperature was evaluated using isochronal annealing test consisting of incremental heating from 25 to 500 °C with a step of 25 °C and isothermal holding at each temperature for 15 min. The hardness was measured after samples were cooled to room temperature and hardness results were graphically presented as a function of annealing temperature. Alloy softening (hardness transition point) represents the maximum temperature above which hardness degrades rapidly. To properly determine this point 2nd derivative method can be used where first the polynomial curve is determined based on the least square

**Table 1 Al-based alloys chemical compositions (wt.%)**

Alloy	Chemical component, wt.%									
	Si	Fe	Cu	Mn	Mg	Zn	Ti	Sr	Other elements	
									Each	Total
F357	6.5-7.5	0.12	0.05	0.03	0.45-0.6	0.05	0.2	0.0	0.05	0.1
A356	6.5-7.5	0.13-0.25	0.1	0.05	0.30-0.6	0.05	0.2	0.0	0.05	0.15
C355	4.5-5.5	0.13	1.0-1.5	0.05	0.50-0.6	0.05	0.2	0.0	0.05	0.15

**Table 2 Mg-based alloys chemical compositions (wt.%) as per ASTM specification B 93/B 93 M-03**

Alloy	Chemical component, wt.%						
	Zn	Y	Nd	Ag	Gd	Other rare earths	Zr
EV31A	0.2-0.5	...	2.6-3.1	...	1.0-1.7	...	Saturated
QE22A	...	...	2.0	2.5	...	...	0.60
ZE41A	3.5-5.0	...	...	...	...	0.8-1.7	0.4-1.0
WE43B	...	3.7-4.3	2.0-2.5	...	...	1.9 max	0.4 min

**Table 3 Summary of Al- and Mg-based alloys processing conditions and testing**

Alloy	Condition	Processing parameters	Testing applied
F357	As-cast T6	Cast into B108 permanent mold ST at 544 °C for 13 h AA at 160 °C for 6 h	DIL, ER, TA, HRF, RTT, ANN, MA
A356	As-cast T6	Cast into B108 permanent mold ST at 538 °C for 13 h AA at 154 °C for 6 h	
C355	As-cast T6	Cast into B108 permanent mold ST at 529 °C for 13 h AA at 154 °C for 7 h	
EV31A	As-cast T6	Cast into B108 permanent mold ST 520 °C for 8 h AA at 200 °C for 16 h	
QE22A	As-cast T6	Cast into B108 permanent mold ST 525 °C for 8 h AA at 215 °C for 4 h	
ZE41A	As-cast T5	Cast into B108 permanent mold AA at 330 °C for 2 h	
WE43B	As-cast T6	Cast into B108 permanent mold ST 525 °C for 8 h AA at 250 °C for 16 h	

*DIL* dilatometer Analysis, *ER* electrical resistivity, *HRB* hardness, *RTT* room tensile testing, *ANN* annealing from 25 to 500 °C experiments, *MA* microstructure analysis, *ST* solution treatment, *AA* artificial aging, *TA* thermal analysis

method using the experimental set of hardness data, and next derivative is calculated to determine the transition points. The samples in as-cast and tempered states were in the form of disks, with a diameter and a height of 20 mm. An air circulating resistant furnace (Blue M, Park Thermal), with a temperature accuracy of  $\pm 3$  °C was used. The room temperature uniaxial tensile tests were performed on the as-cast and heat-treated Al and Mg samples following ASTM: E8/E8 M-11 and ASTM: E9-09 standards at a strain rate of  $10^{-3}$ /s using the computerized tensile testing machine.

The microstructure examinations were carried out using an optical microscope and Nova NanoSEM 650 (FETM) Scanning Electron Microscope (SEM). The EDX chemical analyses in the mode of both spot and surface mapping were performed using a 15 kV voltage with background corrections applied to improve the quantification accuracy of minor elements. To quantify results, at least four different locations were analyzed on each phase and the mean and standard deviation values were calculated.

## 2.2 Assessment of Thermo-physical Properties

The BÄHR DIL 805A/D quench dilatometer was used for analysis of aging kinetics during isochronal heating of as-cast and tempered alloys from 25 to 500 °C with a heating rate of  $\sim 0.1$  °C/s. The cylindrical samples with a diameter of 5 mm and a gage length of  $L = 10$  mm were used in dilatometric studies. The sample length change ( $dL$ ,  $\mu\text{m}$ ) and its derivative curves ( $dL/dt$ ,  $\mu\text{m/s}$ ) were calculated and plotted as a function of testing temperature. Continuous heating of a saturated solid solution results in precipitation of dissolved solute, what increases the sample length. Dissolution of precipitates, on the other hand, decreases the sample length (Ref 11, 12). The typical peak curve shape could be described by key characteristic points, i.e., beginning of the peak and maximum of the peak followed by a subsequent peak minimum. Such a peak

represents an energy signature of aging transformation reactions occurring during testing. Within the scope of this work, the over-aging temperature was considered as beginning of the peak and this point can be linked to the critical-service temperature of the alloy casting. When the latter is exceeded, the component mechanical properties rapidly deteriorate due to precipitate coarsening, resulting in a loss of the precipitate coherency with the alloy matrix (Ref 14).

To complement the dilatometer analysis of aging kinetics, the studies of electrical resistivity were conducted during continuous isochronal heating from 25 to 450 °C for alloys in the as-cast and tempered conditions. The rectangular test samples had dimensions of  $2 \times 2 \times 60$  mm. A four-point method of measuring a potential drop across the sample was used. The potential and the current leads were spot welded to a sample and measurements of potential drops were performed continuously during heating by reversing the known current flowing through the circuit. A detailed description of the technique is given in Ref 11.

## 3. Results and Discussion

### 3.1 Methodology for Evaluation of the Alloy Hardness Retention and Corresponding Phase Transformation Kinetics

The dilatometry experiments were conducted during isochronal heating cycles to detect and analyze the corresponding phase transformation kinetics. An example of the chart showing behavior of the C355-modified alloy (Al-Si-Cu-Mg) in the (i) as-cast, (ii) T6 peak-aged, and (iii) T7 over-aged condition subjected to the dilatometer analysis, is shown in Fig. 1. All analyzed alloys in both the as-cast and T6 conditions exhibited the linear change upon heating as seen in the  $dL$  versus

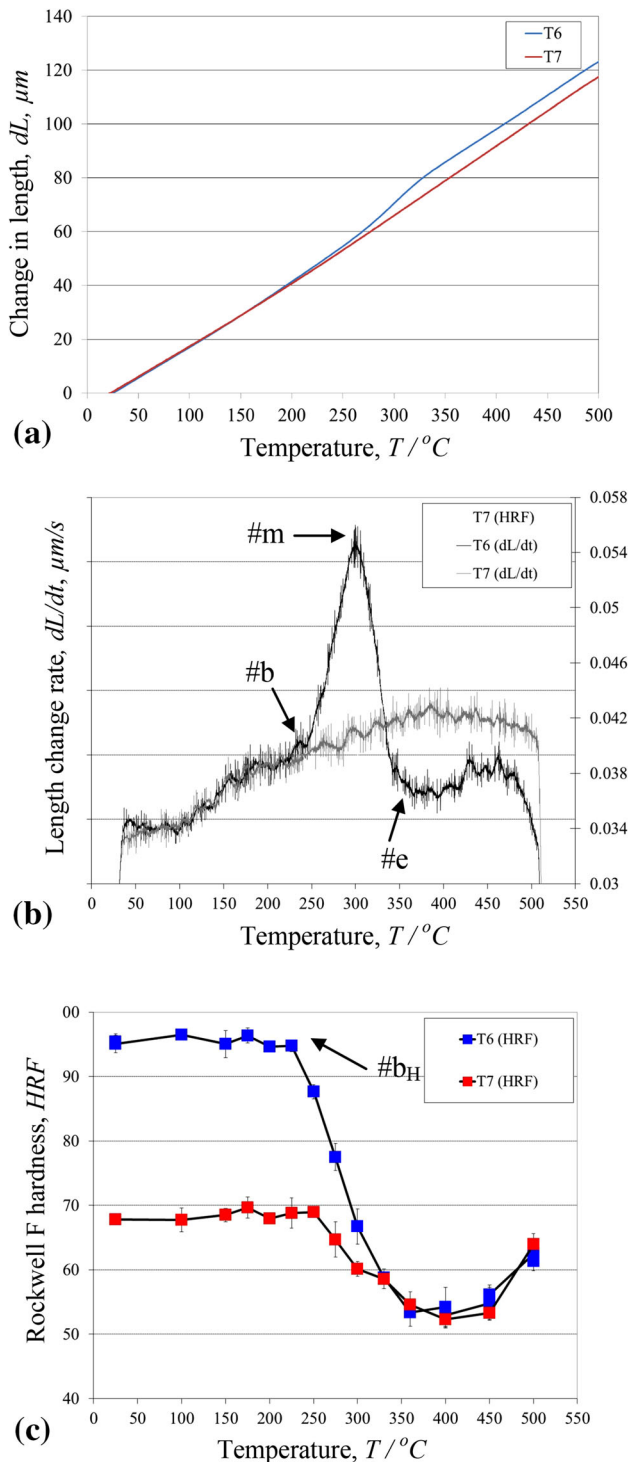


**Fig. 1** Methodology for determination of critical temperature the alloy can withstand without drastic loss of mechanical properties based on dilatometer and hardness measurements carried out for experimental Al-Si-Cu-Mg-based alloy in the as-cast, T6 peak-aged, and T7 over-aged conditions (Ref 4, 37). (a) Length change ( $dL$ ) vs. temperature, (b) length change rate ( $dL/dt$ ) vs. temperature, (c) hardness (HRF) vs. temperature. Note that #b, #m, and #e represent “beginning”, “maximum”, and “end” of the transformation peak, respectively (b), while #b<sub>H</sub> points out hardness transition temperature (c)

temperature curves in Fig. 1(a). The derivative curve ( $dL/dt$ ), as a function of temperature shows distinct transformation peak between temperature points #b and #e, with the maximum at point #m (Fig. 1b). The observed transformation peak on  $dL/dt$  curve is overlaid with the linear expansion effect due to the temperature increase. At temperature point #e,  $dL/dt$  drops to its initial value observed before transformation. Almost constant value of  $dL/dt$  beyond the point #e, indicates completion of the precipitation reactions and the increase of the sample length with temperature occurs due to thermal expansivity of the alloy. The corresponding hardness profile obtained from isochronal heating experiments is presented in Fig. 1(c). The comparison indicates that the beginning of the transformation peak obtained from dilatometer analysis marked as point #b in Fig. 1(b), corresponds to the hardness transition point, marked as point #b<sub>H</sub> in Fig. 1(c).

The  $dL/dt$  peak characteristics, which include peak height and peak location, are controlled by the degree of saturation of solid solution achieved after a given heat treatment. For example, T6 sample upon reheating to 450 °C showed clear transformation peak, while over-aged sample (T7 condition) showed monotonic increase of  $dL/dt$  over corresponding temperature interval. This indicates a lack of phase transformation process upon reheating of T7 sample and the length change occurs due to the alloy thermal expansion without contribution from precipitation or dissolution reactions (Fig. 1b). The resolution of the linear variable displacement transducer (LVDT) used in the dilatometer system (0.05  $\mu\text{m}/0.05^\circ\text{C}$  ( $dL/dT$ )) was sufficient to detect all phase transformation events associated with dimensional changes in the samples, as discussed in the next paragraph.

### 3.2 Characteristics of Al- and Mg-Based Alloys

The properties of both groups of Al and Mg alloys in as-cast and heat-treated states, including the room temperature hardness, tensile properties, and alloy solidification characteristics have been studied. The results permitted to analyze a relationship between the room temperature properties and the hardness retention during high-temperature exposures.

**3.2.1 Melting and Solidification Characteristics.** Thermal analysis experiments during heating and cooling cycles were conducted to understand melting and solidification characteristics required to establish alloys’ processing parameters during ingot melting and casting (Ref 13). The charts summarizing a key thermal data including solidus and liquidus temperatures during melting and solidification are shown in Fig. 2. The liquidus temperature of Mg alloys is generally higher than that of Al alloys, approaching 650 °C for EV31A and up to 620 °C for C355 alloy (Fig. 2a). In contrast, melting/solidification temperature of the eutectics is consistently higher in Al alloys. Although the solidus temperature during solidification cycle of Mg alloys strongly depends on the alloy grade, it falls in the same range of temperatures as measured for Al alloys (Fig. 2b).

**3.2.2 Phase Composition and Microstructure.** The Al alloys A356 and F357 have the same composition limits for Si and Fe, but the latter has half of Cu and higher Mg content. The C355 alloy contains less Si (i.e., 4.5-5.5%), has more Cu than both the A356 and F357 grades (i.e., 1.5 versus 0.1 and 0.05%, respectively) and its Mg content range is between that of A356

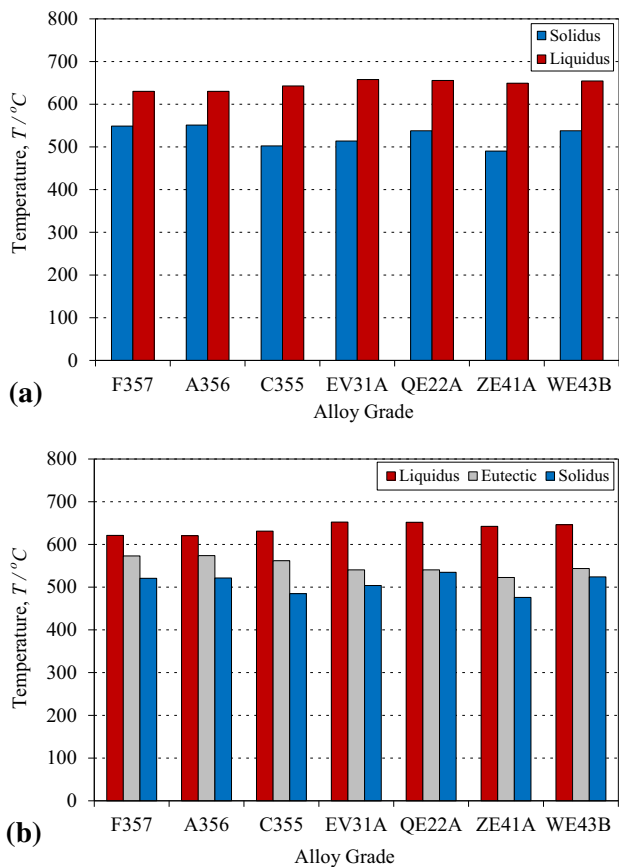


**Fig. 2** Thermal analysis results for Al and Mg Alloys obtained during: (a) melting cycle to 750 °C with 0.2 °C/s heating rate, (b) solidification cycle from 750 °C with 0.1 °C/s cooling rate. Note that  $T_{\text{liquidus}}$ ,  $T_{\text{solidus}}$ , and  $T_{\text{eutectic}}$  melting temperatures are presented. The difference between liquidus and solidus temperature represents alloy solidification range interval

and F357. In all Al alloys studied, Si is the major alloying element, added to improve castability (Ref 15, 16). In addition, Si improves wear resistance due to formation of the Al-Si eutectics. The plate-like Al-Si eutectics, observed after casting, undergoes morphological changes during solutionizing treatment resulting in a fibrous structure. The degree of the eutectic Si modification depends on addition of Sr, solidification rate, and parameters of the solution treatment (Ref 17-21). The difference between the as-cast and T6-tempered microstructures of the C355 alloy is presented in Fig. 3.

It is known that the more fibrous the Si phase is, the better the tensile properties should be expected (Ref 12). In Al alloys, Mg is responsible for solution strengthening of the Al matrix and after aging it forms the  $\text{Mg}_2\text{Si}$  intermetallics (Ref 15, 17, 18). It is generally accepted that the precipitation sequence is as follows  $\text{SSS} \rightarrow \text{GP zones} \rightarrow \beta'' \rightarrow \beta' + \text{Si} \rightarrow \beta\text{-Mg}_2\text{Si}$  (Ref 22). Based on TEM study by Li et al. (Ref 23), the equilibrium precipitate composition is  $\text{Mg}_2\text{Si}$ .  $\text{Mg}_2\text{Si}$  forms at 457 °C in the unrefined A356 alloy and at 465 °C in the A356 alloy refined with 2.5% Al-5Ti-B master alloy (Ref 22). The Cu additions introduce  $\theta\text{-Al}_2\text{Cu}$  as the main strengthening phase (Ref 21), increase the heat treatment response (Ref 16, 21), and decrease the corrosion resistance (Ref 16, 19). Additions of Fe form the rod-like  $\beta$ -phase  $\text{Al}_5\text{FeSi}$  and can be detrimental to ductility as well as to strength (Ref 15, 24). With Mn addition,

the plate-like  $\alpha$ -phase  $\text{Al}_{15}(\text{Fe},\text{Mn})_3\text{Si}_2$  is formed (Ref 15, 24), while if Mg is available in sufficient amount, the  $\pi$ -phase ( $\text{Al}_8\text{FeMg}_3\text{Si}_6$ ) has been observed (Ref 15). The above phases do not dissolve during solutionizing and cannot be reprecipitated in a controlled manner during aging operations (Ref 15, 17, 24). This reduces the Mg amount available for precipitation hardening via its contribution to  $\text{Mg}_2\text{Si}$ . Additions of Be and Mn are used to minimize the effects of Fe (Ref 15, 16), while Ti is being added to reduce the size of the  $\alpha$ -Al grain (Ref 15, 22). All Al-based alloys used in the present study had the same nominal concentration of Ti, so they should experience the same degree of grain refinement. Examples of the microstructure of C355 Al alloy after various heat treatment conditions are shown in Fig. 3. The main microstructural constituents are pointed by arrows and the summary of major intermetallic phases observed in the Al-based alloys is listed in Table 4.

The Mg-based alloys studied here are intended for sand cast; specialty aerospace components aimed for high-temperature applications up to 250 °C. Their chemical compositions are based predominantly on additions of Ag, Zr, and Zn as well as rare earth elements such as Y, Nd, or Gd. The combination of alloying elements results in the development of thermally stable microstructure consisting of Mg matrix, Mg eutectics, and various primary and secondary phases containing rare earth elements. The summary of main intermetallic phases observed in Mg-based alloys is presented in Table 5. The EV31A (Elektron 21) is alloyed predominantly by the additions of Nd (2.6-3.1%), Gd (1.0-1.7%), Zn (0.2-0.5%), and Zr in a form of the saturated solid solution (Table 2). The as-cast microstructure consists of  $\alpha$ -Mg solid solution and eutectic  $\alpha$ -Mg +  $\text{Mg}_3(\text{Nd}_x, \text{Gd}_{1-x})$  or  $\text{Mg}_{12}(\text{Nd}_x, \text{Gd}_{1-x})$  located at grain boundaries (Ref 25, 26). The latter phases are a modification of  $\text{Mg}_3\text{Nd}$  and  $\text{Mg}_{12}\text{Nd}$ , respectively, and dissolve in the matrix during solution treatment. The eutectic phases are often detected in the as-cast condition on the fracture surface. The EV31A requires T6 tempering with solution treatment at 520 °C for 8 h, followed by quenching in hot water or polymer followed by artificial aging at 200 °C for 16 h (Ref 25).

The QE22A alloy contains additions of 2.0% Nd, 2.5% Ag, and 0.6% Zr which remain in the saturated solid solution. The as-cast microstructure, besides the  $\alpha$ -Mg matrix and Mg eutectics, contains the  $(\text{Mg}_x, \text{Ag}_{1-x})\text{Nd}$  intermetallic phases. The alloy is typically T6 tempered in a treatment consisting of solutionizing at 527-535 °C for 4-8 h and artificial aging at 200 °C for 8-16 h (Ref 19). Barucca et al. (Ref 27) reported 204 °C as the industrially accepted aging temperature that leads to formation of the stable  $(\text{Mg}_x, \text{Ag}_{1-x})_{12}\text{Nd}$  phase.

The WE43 alloy was developed for service at elevated temperatures and it maintains its good mechanical properties for long-term exposures up to 250 °C (Ref 28). Of the two grades WE43A and WE43B, the latter has lower contents of Mn (0.03%) and contaminants such as Cu and Ni. Also total contribution of Zn and Ag is limited to 0.15% (Ref 29). The alloy phase composition depends on aging state and includes phases such as  $\beta''$ ,  $\beta'$ ,  $\beta_1$ , and equilibrium  $\beta$  (Ref 30). After aging at temperatures from 175 to 300°, the  $\beta'$ -phase ( $\text{Mg}_{12}\text{NdY}$ ) forms, which is common when the treated alloy is exposed to temperatures equal to or greater than 300 °C. The  $\beta_1$  and  $\beta'$  phases eventually become the  $\beta$  phase having, in the WE43 alloy, a stoichiometry of  $\text{Mg}_{14}\text{Nd}_2\text{Y}$  (Ref 31). An example of the microstructure of the WE43B alloy in the as-cast and tempered condition is shown in Fig. 4.

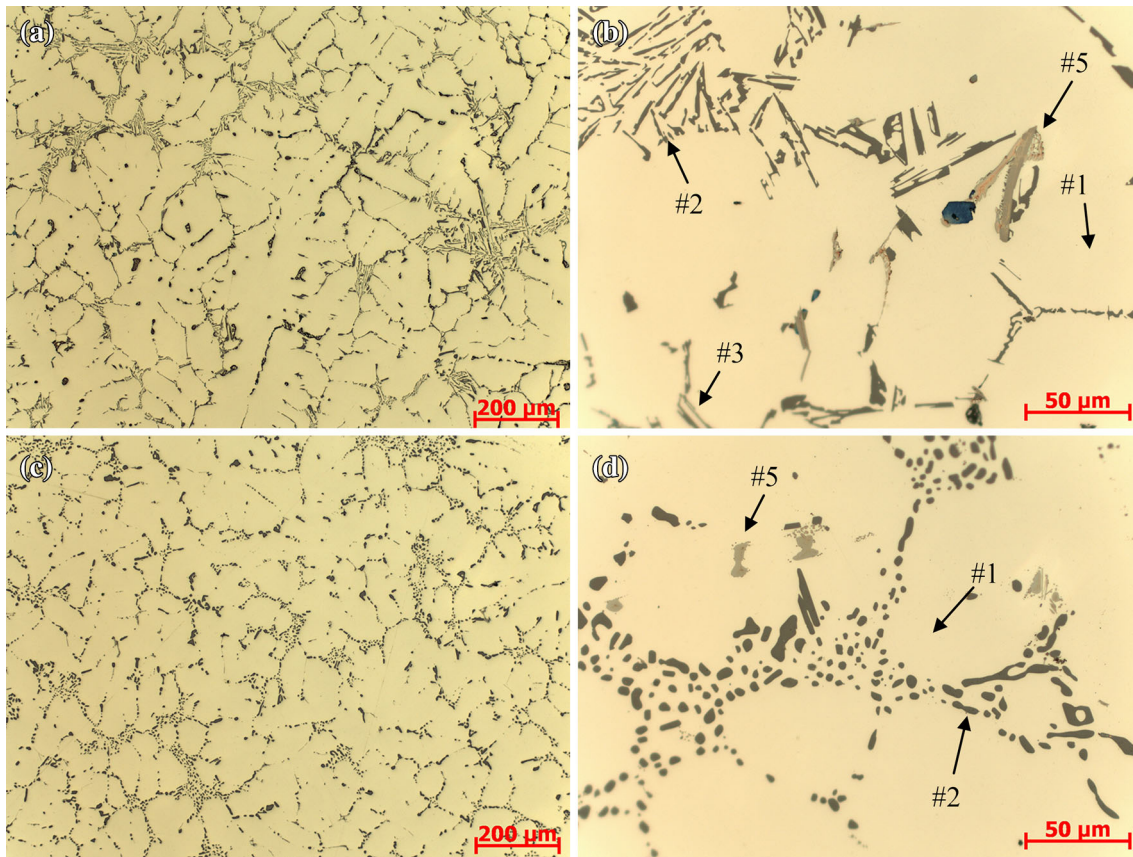


**Fig. 3** Optical microstructure of C355 Al-based alloy under  $\times 100$  and  $\times 500$  magnification in the following conditions: (a, b) as-cast, (c, d) T6 heat treated. Note that selected phases are depicted by numbered arrows and are summarized in Table 4

**Table 4** Summary of intermetallic phases observed in the investigated Al-based alloys (Ref 16)

Alloy	No.	Phase
F357	1	$\alpha$ -Al matrix
	2	Si
	3	$\text{Al}_8\text{Fe}_2\text{Si}$
	4	$\text{Al}_5\text{FeSi}$
	5	$\text{Al}_8\text{Mg}_3\text{FeSi}_6$
	6	$\text{Mg}_2\text{Si}$
A356	1	$\alpha$ -Al matrix
	2	Si
	3	$\text{Al}_8\text{Mg}_3\text{FeSi}_6$
	4	$\text{Mg}_2\text{Si}$
	5	$\text{Al}_5\text{FeSi}$
C355	1	$\alpha$ -Al matrix
	2	Si
	3	$\text{Al}_5\text{FeSi}$
	4	$\text{Al}_8\text{Mg}_3\text{FeSi}_6$
	5	$\text{Al}_5\text{Mg}_8\text{Cu}_2\text{Si}_6$
	6	$\text{Al}_2\text{Cu}$
	7	$\text{Mg}_2\text{Si}$

**Table 5** Summary of intermetallic phases present in the investigated Mg-based alloys (Ref 32)

Alloy	No.	Phase
EV31A	1	$\alpha$ -Mg
	2	$\alpha$ (Mg)- $\beta$ ( $\text{Mg}_{17}\text{Al}_{12}$ ) eutectic
	3	$\text{Mg}_3(\text{Nd}_x, \text{Gd}_{1-x})$
	4	$\text{Mg}_{12}(\text{Nd}_x, \text{Gd}_{1-x})$
	5	$\text{Mg}_3\text{Nd}$
	6	$\text{Mg}_{12}\text{Nd}$
QE22A	1	$\alpha$ -Mg
	2	$\alpha$ (Mg)- $\beta$ ( $\text{Mg}_{17}\text{Al}_{12}$ ) eutectic
	3	$(\text{Mg}_x, \text{Ag}_{1-x})_{12}\text{Nd}$
WE43B	1	$\alpha$ -Mg
	2	$\alpha$ (Mg)- $\beta$ ( $\text{Mg}_{17}\text{Al}_{12}$ ) eutectic
	3	$\text{Mg}_{14}\text{Nd}_2\text{Y}$
ZE41A	1	$\alpha$ -Mg
	2	$\alpha$ (Mg)- $\beta$ ( $\text{Mg}_{17}\text{Al}_{12}$ ) eutectic
	3	B-Mg-Zn-RE
	4	$\text{Mg}_7\text{Zn}_3\text{RE}$

The ZE41A alloy is typically used after T5 heat treatment (Ref 32). The as-cast microstructure consists of eutectics surrounding the  $\alpha$ -Mg grains, like in as-cast EV31A and QE22A grades. In the ZE41A alloy, the eutectics show visibly higher volume fraction and according to Riddle et al. (Ref 33),

it is built of  $\alpha$ -Mg and  $\beta$ -Mg-Zn-RE. More recent literature describes the eutectic structure having  $\text{Mg}_7\text{Zn}_3\text{RE}$  as the secondary phase (Ref 32-35). This corresponds to the Mg and Zn content of 64 and 27 at.%, respectively. Aging for 2 h at  $329 \pm 6$  °C results in satisfactory mechanical properties, which can be further improved by a thermal treatment for 16 h at  $177 \pm 6$  °C (Ref 34). Based on Lagowski's findings (Ref 36),

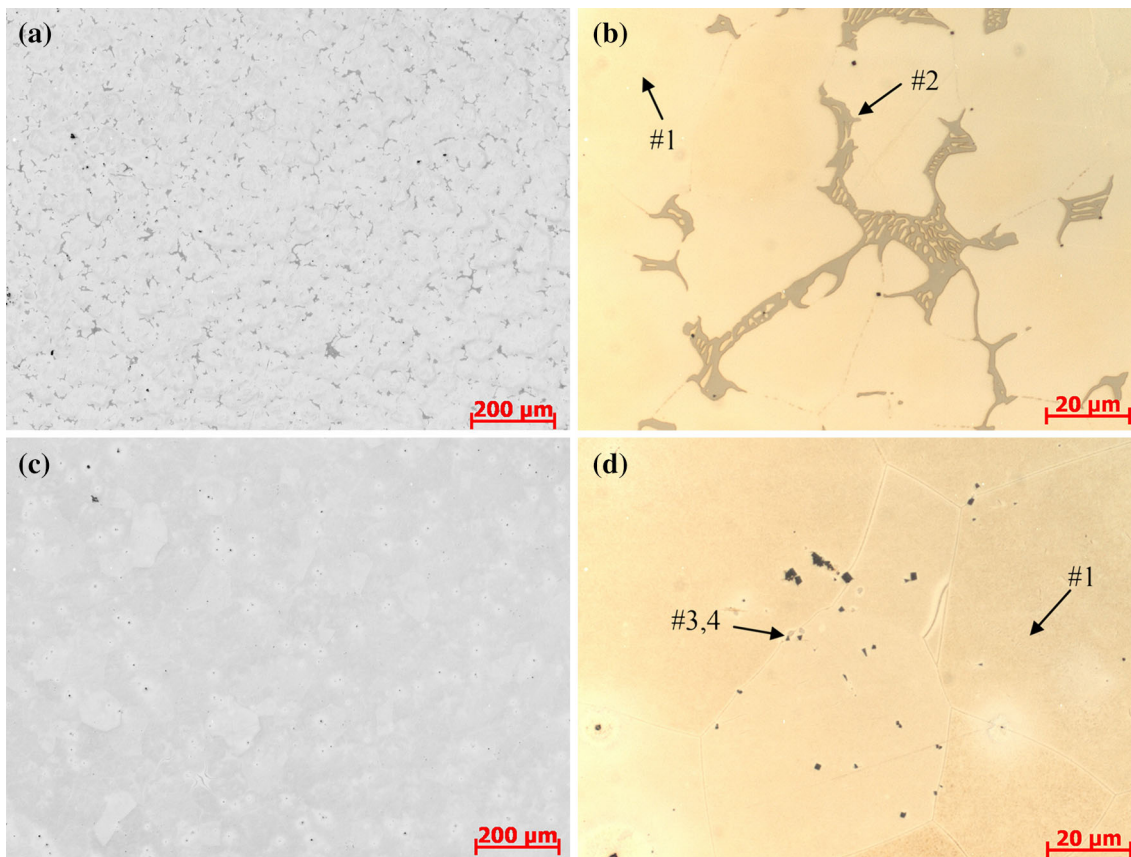


**Fig. 4** Optical microstructure of WE43B Mg-based alloy under  $\times 100$  and  $\times 500$  magnification in the following conditions: (a, b) as-cast, (c, d) T6 heat treated. Note that selected phases are depicted by numbered arrows and are summarized in Table 5

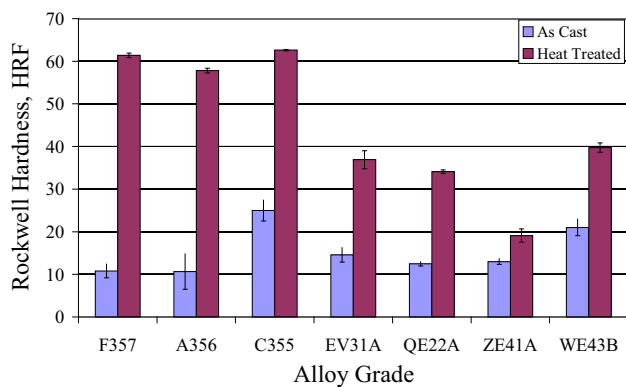


**Fig. 5** As-cast and T6 hardness of the Al and Mg-based alloys. Note similar hardness for all alloys in the as-cast condition and approximately twice higher hardness for Al-based alloys in the tempered condition. Higher hardening response for Al-based alloys is visible

the YS, UTS, and elongation of the heat-treated alloy in this experiment are very close to those obtained after aging at  $330\text{ }^{\circ}\text{C}$  for 2 h followed by 72 h at  $120\text{ }^{\circ}\text{C}$ .

**3.2.3 Hardness and Tensile Properties.** The hardness is commonly being used as an indicator of the alloy's high-temperature performance since it can be correlated with other mechanical properties. The room temperature hardness of Al alloys in tempered conditions showed similar level with the highest value of  $62.6 \pm 0.15$  HRF for C355, followed by

$61.4 \pm 0.5$  HRF for F357, and the lowest value of  $57.8 \pm 0.5$  HRF for A356 (Fig. 5). While hardness differences remained small, they were statistically significant. A similar trend was observed for as-cast condition with C355 having the highest hardness of  $24.9 \pm 2.4$  HRF among all analyzed alloys. The age-hardening response, i.e., the difference between hardness in the as-cast and heat-treated conditions was approximately 600% for F357 (10.7 versus 60.3 HRF) and A356 (10.6 versus 57.8 HRF) and 250% for C355 (24.9 versus 62.6 HRF) alloy. The as-cast hardness of Mg alloys does not generally exceed 20 HRF. In contrast to Al alloys, T6/T5 heat treatment of Mg alloys exerts much lower effect. The EV31A and QE22A grades reached a similar hardness of  $36.8 \pm 2.1$  and  $34.1 \pm 0.4$  HRF, respectively, in the T6 condition, while the WE43B had the highest hardness of  $39.7 \pm 1.1$  HRF. The substantially lower hardness of  $19.1 \pm 1.9$  HRF was measured for the ZE41A alloy.

The tensile strength in as-cast state was similar for all Al and Mg alloys with values between approximately 170 and 205 MPa (Fig. 6a). A similar trend was exhibited by yield stress with values between about 100 and 150 MPa. There was a difference in elongation, which for as-cast state was substantially higher for Mg alloys. In case of the EV31A grade the elongation reached 8%, being twice of that seen for Al alloys.

As expected, T6 heat treatment led to substantial increase in strength and yield stress of Al alloys (Fig. 6b). The C355 alloy developed the highest strength of  $341 \pm 1.9$  MPa, yield stress of  $247 \pm 0.7$  MPa, and elongation of  $6.2 \pm 0.02\%$ . The observed differences between Al alloys in the as-cast and T6

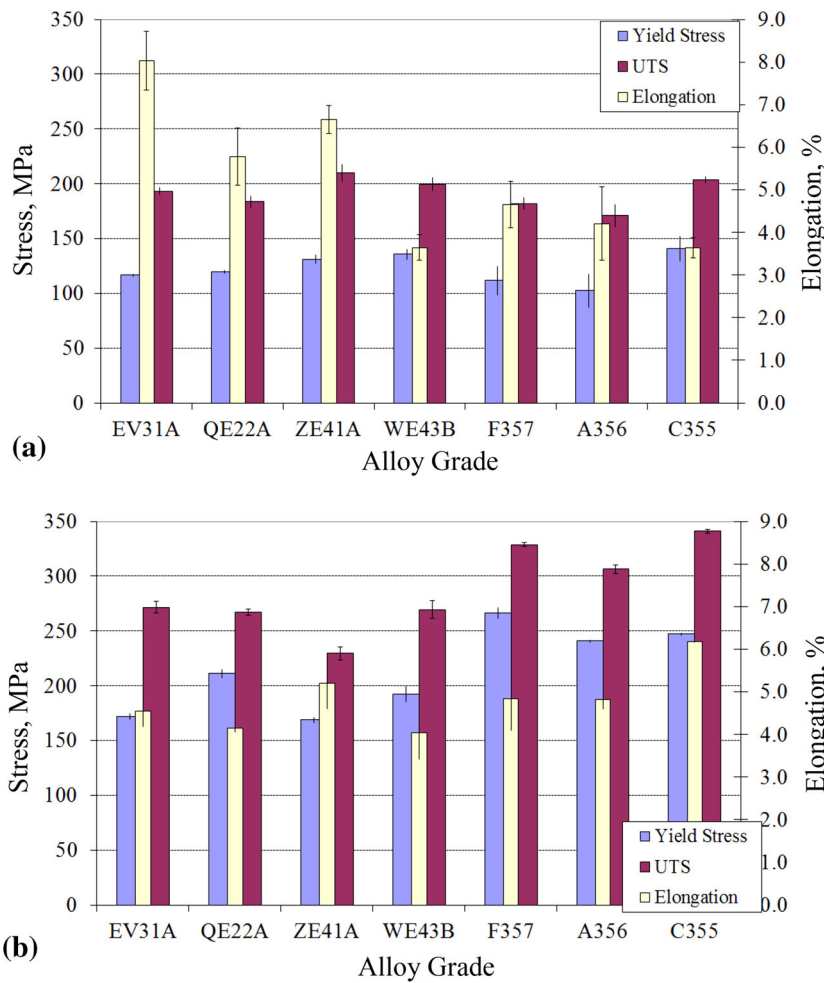


**Fig. 6** As-cast (a) and T6 (b) tensile characteristics of the Al- and Mg-based alloys. Note rather similar values of YS and UTS between Al- and Mg-based alloys except higher E for Mg-based alloys in the tempered condition

conditions varied between 5 to 10% and were statistically significant. The strengthening response was up to 50%, depending on the alloy grade.

For Mg alloys, T6/T5 heat treatment led to tensile strength between 230 and 271 MPa, yield stress between 168 and 211 MPa and elongation between 4 and 5%. The highest strength of  $271 \pm 5.3$  MPa in the tempered condition reached the EV31A alloy, with yield stress of  $172 \pm 3.0$  MPa and elongation of  $4.5 \pm 0.3$  MPa. The lowest strength of  $229 \pm 6.1$  MPa in the tempered condition was observed for ZE41A alloy, having yield stress of  $167 \pm 2.6$  MPa. Its elongation of  $5.2 \pm 0.6\%$ , however, was the highest among all Mg alloys. The strengthening response of Mg alloys was up to 40% depending on the alloy grade.

### 3.3 Hardness Retention After High-Temperature Exposures and Corresponding Phase Transformations

**3.3.1 Al-Based Alloys.** The analysis of hardness as a function of testing temperature revealed that T6 heat-treated A356 and F357 alloys show steady hardness retention of approximately 95 HRF from room temperature up to 225 and 220 °C, respectively (Fig. 7a). When the temperature of 225 or 220 °C was exceeded, the transitional hardness drop was observed from approximately 90 to 30 HRF and 95 to 33 HRF

for A356 and F357 alloys, respectively. The C355 alloy after T6 treatment exhibited higher hardness retention since softening was shifted from 220 to 238 °C and resulted in hardness decrease from approximately 97 to 50 HRF. The hardness retention between temperature range of 325–450 °C was statistically higher for C355 alloy as compared with A356 and F357, i.e., approximately 55 HRF and 30 HRF, respectively (Fig. 7a). Since C355 alloy has the higher content of primary intermetallic phases they, most likely, contribute to higher hardness retention at elevated temperatures. The room temperature hardness measurement in the as-cast condition showed that the C355 alloy had the highest value out of all analyzed alloys. In addition, it was observed that the C355 alloy experienced the lower hardness loss after exposure to temperatures between 225 and 325 °C and higher hardness value after exposure in the temperature range of 325–450 °C.

In the tempered condition, the temperature of 220, 225, and 238 °C, corresponding to the over-aging reaction, has been established as the transition temperature above which degradation of hardness was observed for F357, A356, and C355 grades, respectively (Fig. 7a). As simplified approach, this transition temperature can be derived by finding out the intercept point of the two tangent lines plotted to the plateau and descending part of the hardness curve. As compared with



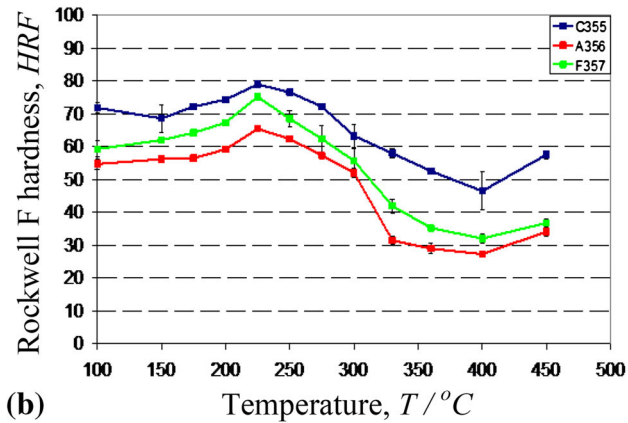
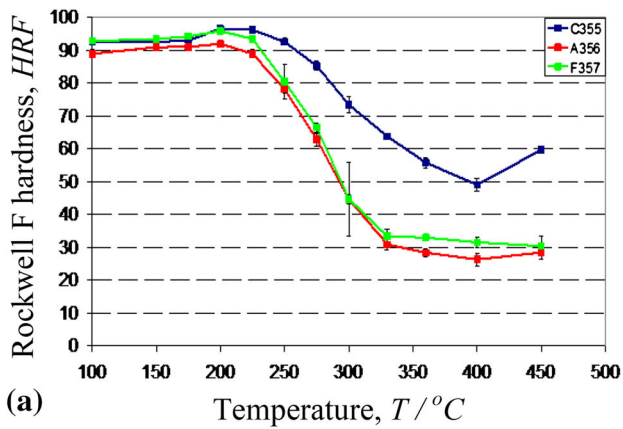


**Fig. 7** Change in hardness of C355, A356, and F357 Al-based alloys as a function of annealing temperature between 100 to 450 °C obtained for the following conditions: (a) T6, (b) as-cast. Note higher hardness for C355 alloy for both conditions, while A356 and F357 starts to soft approximately at 225 and 220 °C while C355 at approximately 238 °C (a). Note lower rate of hardness degradation (slope tangent) for C355 alloy and up to 60% higher hardness between 325 to 450 °C

the as-cast condition (Fig. 7b), all T6-tempered Al alloys showed significant hardening response with about 20% hardness gain from 55 to 72 HRF range to approximately 95 HRF within temperature range from 25 to 225 °C (Fig. 7b). The shape of the hardness curve remained similar for all analyzed alloys without significant difference in the transition temperature where hardness degradation occurred. The as-cast samples taken for all analyzed alloys experienced initial hardness increase, for example for A356 alloy from approximately 55-65 HRF between 25 to 225 °C, followed by transitional decrease to 30 HRF at 325 °C (Fig. 7b). This indicates that some hardening took place upon reheating and some degree of solid solution saturation remained after the sample casting process.

The dilatometer and electrical resistivity analyses were conducted during isochronal heating cycles to detect any potential transformation reactions to develop subsequent correlations with hardness characteristics. While electrical resistivity was done for both groups of alloys, detailed  $dR/dT$  versus temperature data was presented for Mg alloys only since the magnitude of their phase transformation was weaker as compared with Al-based alloys. The superimposed hardness characteristics after exposure at temperatures from 25 to 450 °C and corresponding dilatometer isochronal aging curves for

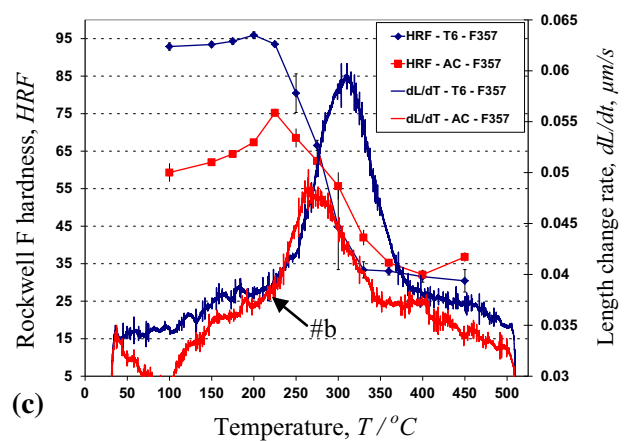
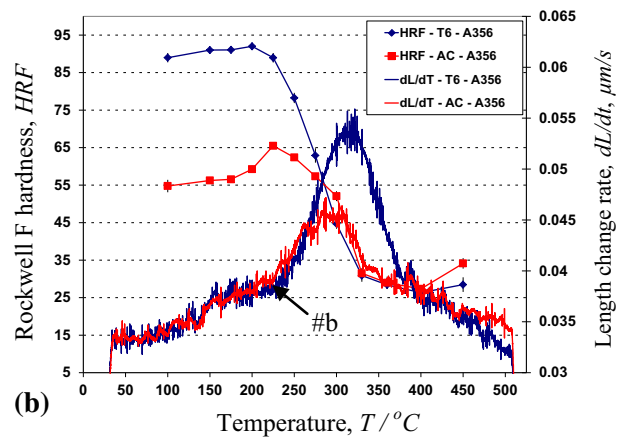
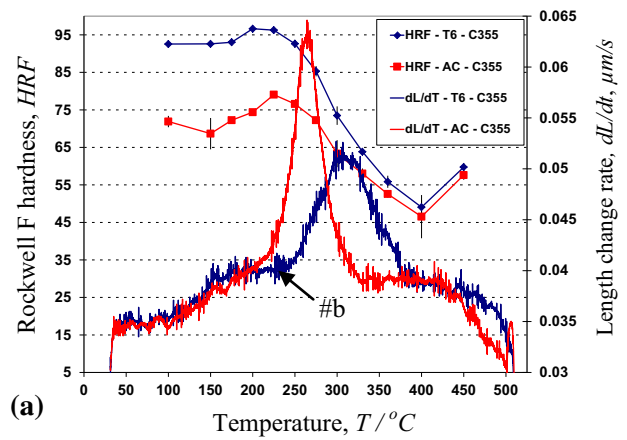


**Fig. 8** Hardness and corresponding phase transformation obtained from dilatometer length change rate measurements collected during isochronal heating from 100 to 500 °C for C355, A356, and F357 alloys in the as-cast and tempered conditions. Note that characteristic points are marked accordingly to the methodology as described on Fig. 1

A356, F357, and C355 alloys in the as-cast and T6-treated conditions are shown in Fig. 8. For all analyzed alloys the beginning of phase transformation, recorded on dilatometer  $dL/dt$  curve (#b), relates to the transition temperature where hardness degradation occurred. While height of the transformation peak observed for the investigated alloys varied, the beginning of the peak between 220 and 238 °C depending on the alloy, matched the hardness transition temperature. Subse-

quently, it was observed that the end of the phase transformation peak, i.e., 400 °C Fig. 1(b) point (#) matches the hardness curve plateau, where no hardness increase was observed. Similar observations were confirmed for as-cast and T6-tempered conditions. The only difference in the hardness characteristics between analyzed alloys was that the C355 alloy had the higher peak hardness in the temperature range from 100 to 225 °C, less steep hardness loss between 225 and 325 °C, and higher hardness between 325 and 450 °C, as compared with A356 and F357 alloys.

**3.3.2 Mg-Based Alloys.** The investigated Mg alloys in the tempered condition did not show abrupt hardness changes over the testing temperature range, instead the hardness loss was gradual or even constant along the testing temperature interval from 25 to 450 °C (Fig. 9a). The ZE41A alloy in the T5-tempered condition had almost the same hardness at the level of approximately 70 HRF throughout entire temperature range. The QE22A and EV31A alloys exhibited transitional hardness decrease from approximately 80 HRF at 100 °C to 59 HRF at 450 °C that occurred between 225 and 250 °C, respectively. Similar transition in hardness was observed for WE43B alloy at approximately 250 °C but was minor by several units only i.e., from 81 to 75 HRF.

As compared with the as-cast condition, all T6/T5-tempered Mg alloys showed on average approximately 15% hardness increase, i.e., the hardness varied between 60 and 70 HRF to 70-82 HRF at 100 °C and between 55-70 to 59-76 HRF at 450 °C for as-cast and T6 condition, respectively. Hardness changes as observed at temperatures from 25 to 450 °C for alloys in the as-cast condition had different characteristics than heat-treated alloys. In contrast to Al alloys, the as-cast Mg alloys did not show visible aging effect manifested by peak hardness observed when ramping the as-cast test samples from 25 to 450 °C (Fig. 9b). The QE22A was an exception from this behavior, showing as-cast hardness increase from approximately 60 HRF at 100 °C to 73 HRF at 250 °C followed by the gradual decrease down to 55 HRF at 450 °C.

The EV31A and WE43B alloys showed distinct transformation peaks identified using both the dilatometer and electrical resistivity methods (Fig. 10b and d, 11b and d). The QE22A alloy showed the transformation peak, the beginning of the peak at 250 °C was rather minor since it was observed only by electrical resistivity measurements (Fig. 11a). The EV31A alloy had the transformation peak with beginning at approximately 255 °C and maximum at 300 °C followed by subsequent minimum at 330 °C as detected using the dilatometer (Fig. 10b) and electrical resistivity measurement (Fig. 11b). Some discrepancy existed between electrical resistivity and dilatometer measurements as far as temperature of transformation peaks is concerned. The superimposed hardness and transformation kinetics data as obtained from dilatometer (Fig. 10b) and electrical resistivity (Fig. 11b) analysis for EV31A alloy showed that transitional hardness change coincides with beginning of the transformation peak at approximately 255 °C (Fig. 10b, point #b). This phenomenon was clearly observed for T6 test samples and less clearly for sample in the as-cast condition. The recorded dilatometer peak for the EV31A alloy is associated with sample contraction, the  $dL/dt$  decreased from 0.048 to 0.033  $\mu\text{m/s}$  over the temperature range from 280 to 330 °C (Fig. 10b). The contraction effect was significant since it exceeded sample expansion during heating. A similar trend was observed for EV31A alloy in phase transformation assessment by electrical resistivity measure-

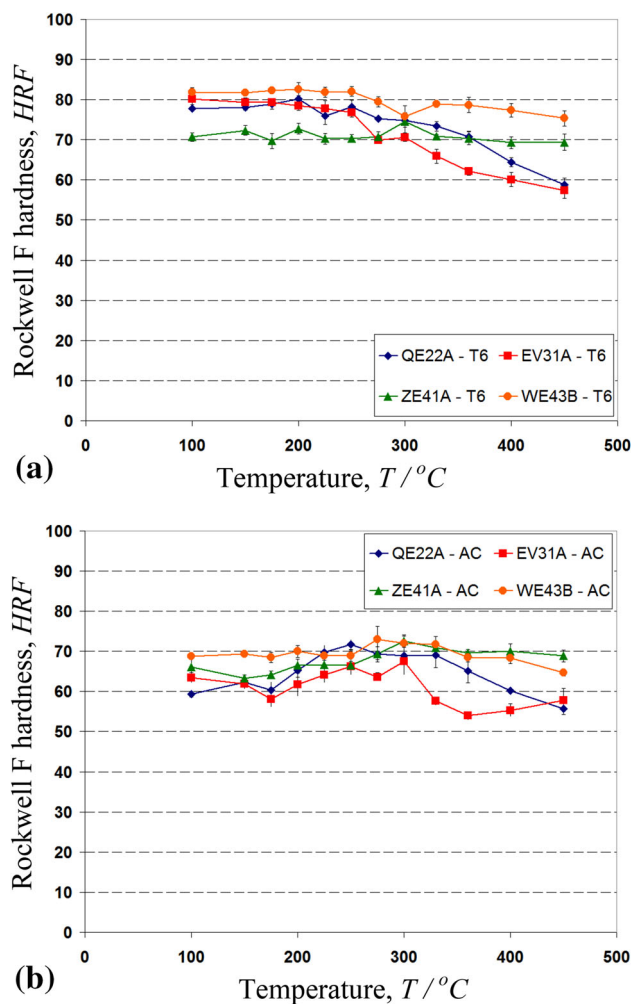


**Fig. 9** Change in hardness obtained for QE22A, EV31A, ZE41A, and WE43B Mg-based alloys as a function of annealing temperature between 100 to 450 °C in the following conditions: (a) T6, (b) as-cast. Note gradual hardness change at approx. 250 °C for WE43B, EV31A and at approx. 225 °C for QE22A, while ZE41A alloy showed steady hardness values over the testing temperature range (~70 HRF) (a)

ments, where the  $dR/dT$  values decreased from 4 to  $-6 \mu\Omega/^\circ\text{C}$  over the temperature range from 280 to 330 °C (Fig. 11b).

The WE43B alloy had a distinct transformation peak as detected by dilatometer analysis, with beginning of the reaction at about 250 °C and maximum at 300 °C, as shown earlier in Fig. 10d. Minor transition hardness degradation over the tested temperature range was observed as seen in this figure. The electrical resistivity analysis carried out for WE43B alloy showed similar results where the distinct transformation peak associated with a dissolution process was clearly manifested by the increase in  $dR/dT$  values from 3 to 11  $\mu\Omega/^\circ\text{C}$  over the temperature range of 280 to 330 °C (Fig. 11d). The QE22A alloy in the T6 condition showed transitional hardness change at 225 °C from 78 to 60 HRF. The corresponding transformation reaction as detected by electrical resistivity measurements was rather minor since it was falling within the background noise not permitting to draw any further conclusions with respect to detailed correlations with hardness characteristics (Fig. 11a). In contrast, the QE22A as-cast alloy showed visible transformation reaction associated with decrease of the  $dR/dT$

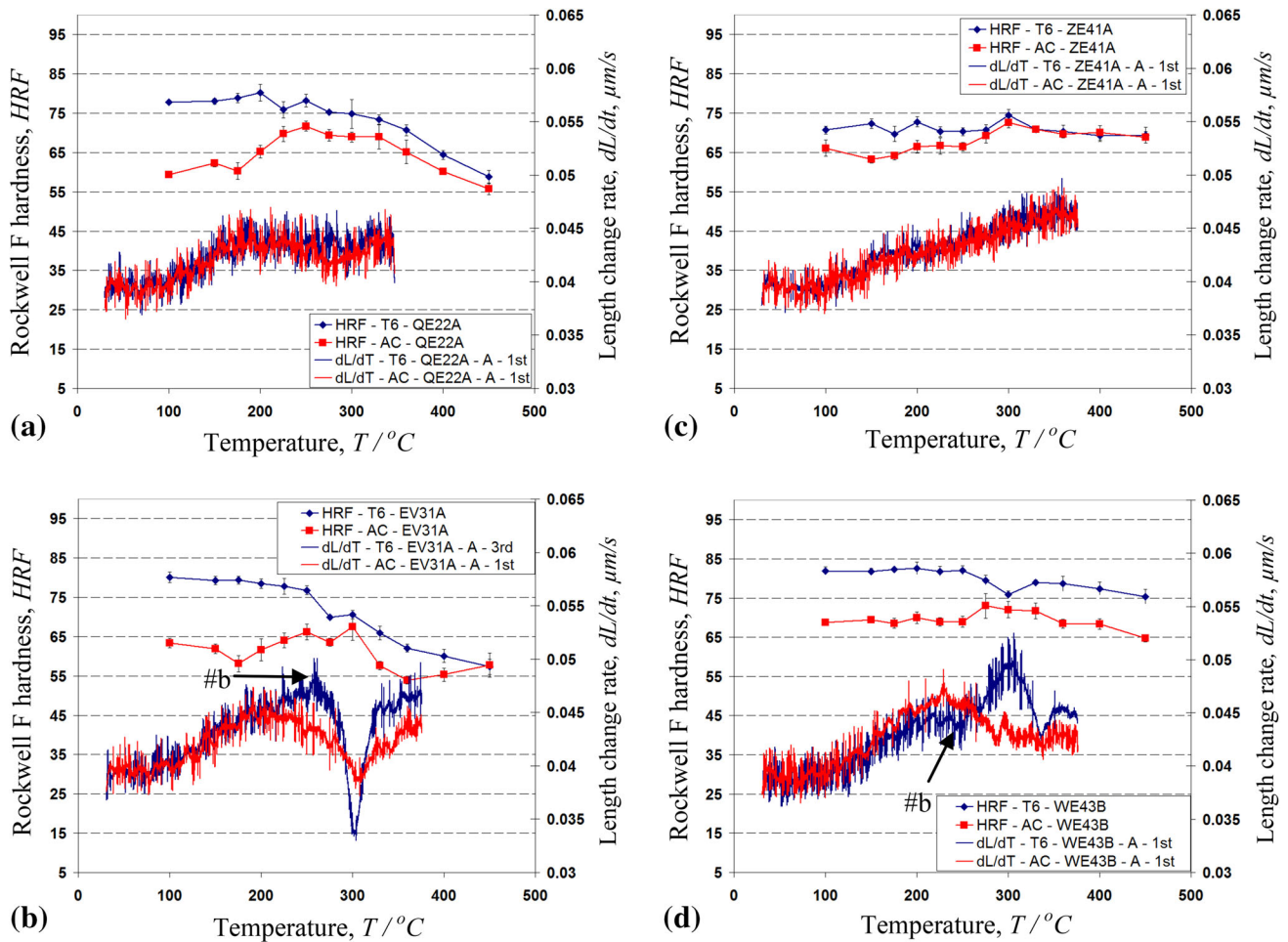


**Fig. 10** Hardness and corresponding phase transformation obtained from dilatometer length rate change measurements ( $dL/dt$ ) for QE22A (a), EV31A (b), ZE41A (c), and WE43B (d) Mg-based alloys in the as-cast, T5 (for ZE41A) and T6 (for remaining alloys) conditions during isochronal heating from 25 to 450 °C. Note lack of visible phase transformation for QE22A and ZE41A, while EV31A showed phases transformation with beginning (#b) at 255 °C associated with alloy contraction, while WE43B had phase transformation with beginning (#b) at 252 °C associated with alloy expansion. Note that characteristic points of transformation peak are marked accordingly to the methodology as described on Fig. 1

values from 2 to  $-1.0 \mu\Omega/\text{C}$  over the temperature range from 280 to 330 °C (Fig. 11a). This transformation was correlated with as-cast hardness increase from approximately 60 HRF at 100 °C to 73 HRF at 250 °C followed by the gradual decrease reaching 55 HRF at 450 °C. This hardness change indicate the strengthening effect associated with precipitation and subsequent dissolution processes. The ZE41A alloy did not show any transformation reaction upon heating of the as-cast as well as T5 heat-treated sample that was confirmed by dilatometer (Fig. 10c) and electrical resistivity (Fig. 11c) analysis. The corresponding hardness values for ZE41A remained almost constant at about 70 HRF for all testing temperatures (Fig. 9a).

In a search for factors affecting the hardness retention temperature, the correlation with initial properties of Mg and Al alloys, measured prior to the isochronal heating experiment, was tested. An example of the relationship between the ultimate tensile strength and hardness retention temperature is shown in Fig. 12. A scatter of data points with a correlation coefficient  $R^2 = 0.183$  indicates a lack of meaningful correlation. Similar outcomes were obtained for other properties including hardness and yield stress. In contrast, the strong correlation was established between hardness degradation temperature and corresponding phase transformation,

understood as beginning of the peak transformation temperature for all Al and Mg alloys analyzed in tempered conditions. This correlation is shown in Fig. 13 where alloys are ranked in the descending order i.e., from the highest to the lowest values of hardness transition temperature. The T5-tempered ZE41A alloy is excluded since its hardness remained constant. On the other hand, the QE22A alloy exhibited the hardness reduction but it did not show corresponding transformation reaction.

The highest value of the hardness degradation temperature of about 250 °C had the EV31A and WE43B followed by C355 alloy with value of 238 °C and QE22A and A356 at 225 °C. The lowest value was recorded for the F357 alloy at 220 °C. The beginning of phase transformation temperature established by the dilatometer analysis matched the hardness measurements with  $\pm 5$  °C while electrical resistivity was correlated with  $\pm 25$  °C. The results indicate that both methodologies are complimentary and dilatometer analysis could be used as stand-alone testing in order to evaluate the transitional softening temperature required for more in-depth estimation of alloys' high-temperature performance.

The comprehensive analysis is required to develop similar correlations between strength degradation at elevated temper-

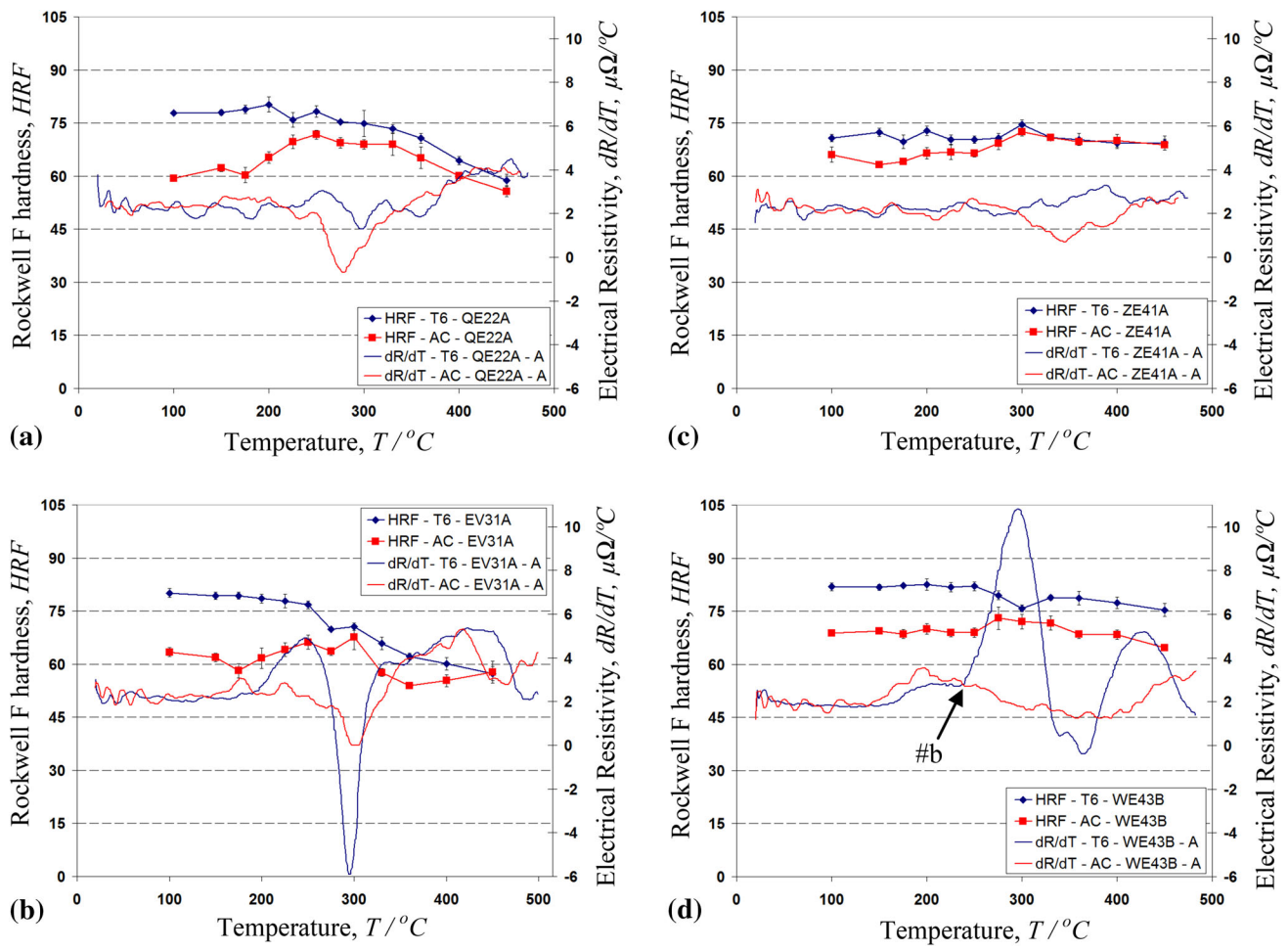


**Fig. 11** Change in hardness and corresponding phases transformation based on electrical resistivity data obtained for QE22A (a), EV31A (b), ZE41A (c), and WE43B (d) Mg-based alloys in the as-cast, T5 (for ZE41A) and T6 (for remaining alloys) conditions during isochronal heating from 25 to 450 °C. Note lack of visible phase transformation for ZE41A alloy (c), while EV31A (b) showed transformation with beginning (#b) at 245 °C related to phase dissolution, while WE43B had visible transformation with beginning (#b) 238 °C related to phase precipitation

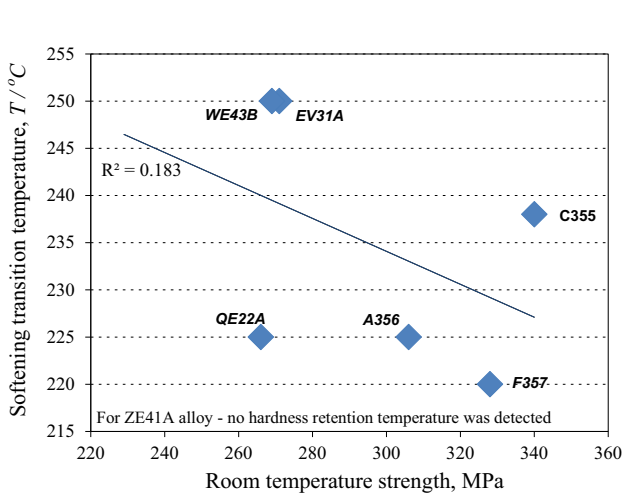


**Fig. 12** Relationship between ultimate tensile strength of Mg and Al alloys in the tempered conditions measured at room temperature prior to isochronal annealing and hardness retention temperature. Note scatter of data points with a correlation coefficient  $R^2 = 0.183$  indicates a lack of meaningful correlation

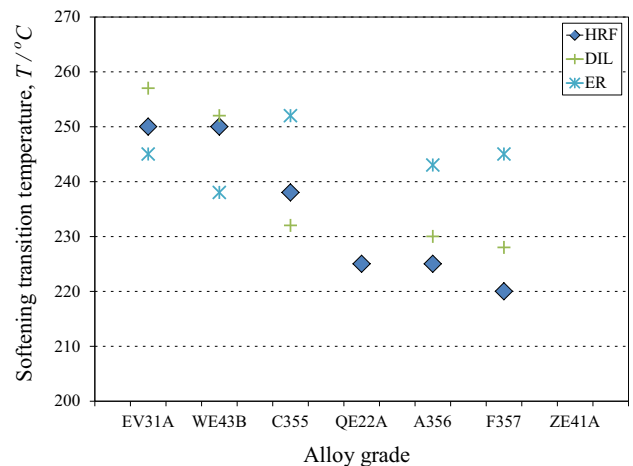


**Fig. 13** Correlation between hardness and dilatometer and electrical resistivity measurements carried out for Al- and Mg-based alloys in the tempered conditions in order to determine the transition temperature where hardness degradation occurs. Close fit between hardness and dilatometer analysis is visible ( $\pm 6$  °C) indicating that such applied techniques could be used interchangeably

ature obtained from tensile/compression testing and corresponding phase transformation. Such a methodology was already outlined in the provisional patent applications and suitable tensile testing equipment configuration was proposed to carry out the simultaneous tensile/compression testing with in situ phases transformation kinetics (Ref 37).

## 4. Conclusions

Two groups of cast Al-based alloys: A356, F357, and C355 and Mg-based alloys: QE22A, EV31A, ZE41A, and WE43B were used to evaluate thermal stability of alloys for applications at elevated temperatures. Both groups of alloys exhibited substantial differences in the hardness retention temperature during annealing up to 450 °C. The Al alloys experienced 34–66% reduction of the initial hardness, which substantially exceeds the hardness reduction of 4–22%, experienced by Mg alloys after the same thermal exposure. For Al alloys the hardness reduction exhibited a steep transition between 220 and 238 °C. In contrast, Mg alloys showed rather gradual hardness reduction, extended to the higher temperatures between 238 and 250 °C.

The as-cast and tempered Al and Mg alloys showed distinct phase transformations upon heating that were detected by dilatometer and electrical resistance measurements. The Al alloys: A356, F357, C355, and Mg alloy WE43B, showed over-aging reactions associated with the alloy expansion, caused by the precipitation process. In contrast, the precipitate dissolution associated with the contraction of the samples was dominant during heating of Mg alloys EV31A and to the lesser extent QE22A alloy. A distinct correlation between the temperature of hardness reduction and the beginning of the phase transformation temperature has been established. This is in contrast to tensile properties and hardness measured prior to isochronal annealing which did not exhibit correlation with temperature of subsequent hardness reduction.

The results suggest that the dilatometric measurements in combination with electrical resistivity measurements represent efficient and powerful methodology to predict the temperature of hardness reduction in commercial Al and Mg alloys. This methodology may be used to determine the suitability of metallic alloys for high-temperature applications in aerospace and/or automotive industry.

## Acknowledgments

Financial support of the Materials for Energy End Use in Transformation Program of Natural Resources Canada is gratefully acknowledged. The authors thank also Marta Aniolek M.Sc. Eng. and Renata Zavadil from CanmetMATERIALS for dilatometer, thermal, and metallographic analysis, Ibrahim Sadiq and Mubashir Mir from the University of Waterloo as well as Pushan Lele from Ryerson University for graphical data representation and literature studies. The authors thank also G. Marzano from Magellan Aerospace Company by providing testing material.

## References

1. R. Nadella, D.G. Eskin, Q. Du, and L. Katgerman, Macrosegregation in Direct-Chill Casting of Aluminum Alloys, *Prog. Mater. Sci.*, 2008, **53**, p 421–480
2. C. Taylor, *Aircraft Propulsion*, Smithsonian Institution Press, Washington, DC, 1971
3. A. Sachdev, R. Mishra, A. Mahato, and A. Alpas, Vehicle Lightweighting: Challenges and Opportunities with Aluminum, *13th International Conference on Aluminum Alloys (ICAA13)*, 2012, p. 609–622
4. W. Kasprzak, B. Amirkhiz, and M. Niewczas, Structure and Properties of Cast Al-Si Based Alloy with Zr-V-Ti Additions and Its Evaluation of High Temperature Performance, *J. Alloys Compd.*, 2014, **595**, p 67–79
5. M. Pekguleryuz and M. Celikin, Creep Resistance in Mg Based Alloys, *Int. Mater. Rev.*, 2010, **55**(4), p 199–217
6. F. Czerwinski, The Oxidation Behaviour of an AZ91D Magnesium Alloy at High Temperature, *Acta Mater.*, 2002, **50**, p 2639–2654
7. M. Hoeschl, W. Wagener, and J. Wolf, BMW's Magnesium-Aluminum Composite Crankcase, State-of-the-Art Light Metal Casting and Manufacturing, SAE Technical Paper 2006-01-0069, 2006, doi: [10.4271/2006-01-0069](https://doi.org/10.4271/2006-01-0069)
8. J. Williams and E. Starke, Progress in Structural Materials for Aerospace Systems, *Acta Mater.*, 2003, **51**, p 5775–5799
9. K. Knipling, D. Dunand, and D. Seidman, Precipitation Evolution in Al-Zr and Al-Zr-Ti Alloys During Aging at 450–600 °C, *Acta Mater.*, 2008, **56**(56), p 1182–1195
10. M. Vlach, I. Stulikova, B. Smolna, N. Zaludova, and J. Cerna, Phase Transformation of Isochronally Annealed Mould-Cast and Cold-Rolled Al-Sc-Zr Based Alloy, *J. Alloys Compd.*, 2010, **492**(1–2), p 143–148
11. M. Niewczas, Z.S. Basinski, S.J. Basinski, and J.D. Embury, Deformation of Copper Single Crystals to Large Strains at 4.2 K: I. Mechanical Response and Electrical Resistivity, *Philos. Mag.*, 2001, **81**, p 1121–1142
12. M. Hafiz and T. Kobayashi, Mechanical Properties and Fracture of Aluminum Casting Alloys, *Int. J. Mater. Prod. Technol.*, 1999, **14**(2–4), p 199–216
13. M. Kasprzak, W. Kasprzak, W. Kierkus, and J. Sokolowski, Method and Apparatus for Universal Metallurgical Simulation and Analysis. US Patent 7,354,491, 2008
14. S. Iwamura, M. Nakayama, and Y. Miura, Coherency Between Al<sub>3</sub>Sc Precipitate and the Matrix in Al Alloys Containing Sc, *Mater. Sci. Forum*, 2002, doi:[10.4028/www.scientific.net/MSF.396-402.1151](https://doi.org/10.4028/www.scientific.net/MSF.396-402.1151)
15. C. Caceres, C. Davidson, J. Griffiths, L. Hogan, and Q. Wang, Hypoeutectic Al-Si-Mg Foundry Alloys, *Mater. Sci. Forum*, 1997, **21**, p 27–43
16. J. Kaufman and E. Rooy, Ed., *Aluminum Alloy Castings—Properties, Processes and Applications*, ASM International, Materials Park, 2004
17. A. Thirugnanam, K. Sukomaran, K. Raghukandan, U. Pillai, and B. Pai, Microstructural Aspects and Fracture Behaviour of A356/357 Alloys—An Overview, *Trans. Indian Inst. Met.*, 2005, **58**(5), p 777–787
18. M. Tiryakioglu and R. Shuey, Quench sensitivity of an Al-7 wt%Si-0.6 wt%Mg alloy: Characterization and Modeling, Simulation of Aluminum Shape Casting Processing: From Alloy Design to Mechanical Properties, *Met. Trans. B*, 2007, **38B**, p 575–582
19. P. Keith, Industrial Heating, *Technovation*, 1997, **64**(2), p 51–57
20. K. Yoshida and R. Arrowood, Microstructure and Mechanical Properties of A356 Aluminum Castings as Related to Various T6-Type Heat Treatments, *Light Weight Alloys for Aerospace Applications III*, E.W. Lee, N.J. Kim, K.V. Jam, and W.E. Frazier, Ed., The Minerals, Metals and Materials Society, Warrendale, 1995, p 77–88
21. C. Caceres, I. Svensson, and J. Taylor, Microstructural Factors and the Mechanical Performance of Al-Si-Mg and Al-Si-Cu-Mg Casting Alloys, *Proceedings of the 2nd International Aluminum Casting Technology Symposium*, ASM International, 1999
22. M. Zhu, G. Yang, and L. Yao, Effect of T6 heat treatment on the microstructures and the aging behavior of the grain-refined A356 alloys, *Adv. Mater. Res.*, 2011, **143**(144), p 1410–1414
23. J. Li, H. Tan, Z. Shi, and Q. He, Analysis of Mg<sub>2</sub>Si precipitates in Al-Si-Mg and Al-Mg-Si alloys by FE-SEM, *Chin. J. Nonferrous Met.*, 2008, **18**(10), p 1819–1824
24. G. Mrowka-Nowotnik and J. Sieniawski, Microstructure and Mechanical Properties of C355.0 Cast Aluminum Alloy, *Arch. Mater. Sci. Eng.*, 2011, **47**(2), p 85–94
25. A. Kielbus, Microstructure and Mechanical Properties of Electron 21 Alloy After Heat Treatment, *J. Achiev. Mater. Manuf. Eng.*, 2007, **20**(1–2), p 127–130

26. A. Kielbus, T. Rzychon, and R. Przeliorz, DSC and Microstructural Investigations of the Elektron 21 Magnesium Alloy, *Mater. Sci. Forum*, 2010, **638–642**, p 1447–1452
27. G. Barucca et al., Formation and Evolution of the Hardening Precipitates in a Mg-Y-Nd Alloy, *Acta Mater.*, 2011, **59**(10), p 4151–4158
28. Elektron WE43—Datasheet 467—Magnesium Elektron, Service and Innovation in Magnesium, [www.magnesium-elektron.com](http://www.magnesium-elektron.com). Accessed 14 May 2014
29. ASTM B93/B93M-03, *Standard Specification for Magnesium Alloys in Ingot Form for Sand Casting, Permanent Mold Casting, and Die Casting*, ASTM International, West Conshohocken, 2003
30. T. Rzychon and A. Kielbus, Microstructure of WE43 Casting Magnesium Alloy, *J. Achiev. Mater. Manuf. Eng.*, 2007, **21**(1), p 31–34
31. B. Smola and I. Stulikova, Equilibrium and Transient Phases in Mg-Y-Nd Ternary Alloys, *J. Alloys Compd.*, 2004, **381**(1–2), p L1–L2
32. M. Avedesian and H. Baker, Ed., *Magnesium and Magnesium Alloys*, ASM International, Materials Park, 1999
33. Y. Riddle, L. Barber, and M. Makhlof, Characterization of Mg Alloy Solidification and As-Cast Microstructure, *Magnesium Technology*, TMS, 2004, pp. 203–208
34. I. Fukui, T. Suzuki, and M. Harada, Characteristics of High Strength Magnesium Casting Alloy QE22A, *Kobe Res. Dev.*, 1982, **32**(2), p 52–55
35. ASTM B80, *Nonferrous Metal Standards and Nonferrous Alloy Standards, Standard Specification for Magnesium Alloy Sand Castings*, ASTM International, West Conshohocken, 2009
36. B. Lagowski and J. Meier, *Properties of Sand-Cast Magnesium Alloys*, Department of Mines and Technical Surveys, Ottawa, 1964
37. W. Kasprzak and M. Niewczas, Method and Apparatus for High Temperature Performance Assessment of Metal Alloys. Patent US Provisional Patent No: 61/512, 565, 2011